RSC Advances

ROYAL SOCIETY OF CHEMISTRY

www.rsc.org/advances

Journal Name

ARTICLE

Comparison of hydrogen, halogen, and tetrel bonds in the complexes of HArF with YH_3X (X = halogen, Y = C and Si)

AReceived 00th January 20xx,
Accepted 00th January 20xx

DOI: 10.1039/x0xx00000x

www.rsc.org/

Mingxiu Liu[a], Qingzhong Li[*,a], Wenzuo Li[a], Jianbo Cheng[a], Sean A.C. McDowell[*,b]

Ab initio MP2/aug-cc-pVTZ calculations were performed in order to find equilibrium structures with Y···F tetrel bonds, X···H hydrogen bonds or X···F halogen bonds on the potential energy surfaces of the complexes formed between HArF and YH_3X (X = halogen, Y = C and Si). For the CH_3X complexes, the hydrogen-bonded complex is the most stable, while the tetrel-bonded complex is the most stable of the SiH_3X complexes. The H–Ar stretch vibration exhibits a red shift for the hydrogen bond but a blue shift for the tetrel and halogen bonds. The hydrogen bonds in the CH_3X and SiH_3X complexes, as well as the tetrel bonds in the SiH_3X complexes, are governed by a combination of electrostatic and polarization energies, exhibiting partially covalent character with negative energy densities and a substantial amount of charge transfer.

1. Introduction

Molecules containing noble gas atoms have attracted much attention because they exhibit distinctive structures and special properties. For instance, the H–Ar stretch vibration of HArF often displays a blue shift when this molecule participates in hydrogen bonds.[1-10] This is in sharp contrast to conventional hydrogen bonds for which a red shift is commonly observed. Moreover, this vibration shows a rather large blue shift when the F atom of HArF forms a halogen bond with dihalogen molecules.[11] Experimenters have tried to synthesize these types of noble-gas molecules using various preparative techniques, most commonly low-temperature matrix-isolation methods.[12-14] Most noble-gas molecules contain a fluorine atom, such as HArF,[12] $XePtF_6$,[15] and KrF_2.[16] On the other hand, there is also much richness and diversity in fluorine-free noble-gas chemistry.[17-19] Most of these noble-gas molecules are metastable in the gas phase and have potentially high reactivity. Consequently, it is a challenge to stabilize these noble-gas molecules in solution.

It has been demonstrated previously that the noble-gas molecules can form stable intermolecular complexes with ordinary molecules.[1-11,20-27] A hydrogen bond is usually involved in the complexes of HNgY, where Ng denotes a noble-gas atom and Y is an electronegative fragment. The molecule HNgY is characterized by both a covalent H-Ng bond and an ionic Ng-Y bond. Interestingly, a blue shift occurs for the H–Ng stretch vibration when it forms a hydrogen bond with small molecules such as H_2, N_2, CO, and CO_2.[1-10] However, the H–Ng stretch vibration shows a red shift when it participates in a hydrogen bond with P_2[23,24] and metal hydrides.[25-27] The HArF molecule can form two stable complexes with dihalogen molecules through a hydrogen bond and a halogen bond, with the halogen-bonded complex being more stable than the hydrogen-bonded counterpart.[11] Moreover, a large blue shift of the H–Ar stretching frequency was found in both complexes, but it amounts to about 200–398 cm^{-1} in the halogen-bonded complex.[11] It was shown that the H–Ng stretching frequency has a dependence on the nature of the noble gas atom.[28,29] For example, the H–Ng stretching frequency has a large blue shift in the π hydrogen-bonded complex C_6H_6-HArF, no shift in the corresponding complex C_6H_6-HKrF, but a small red shift in the corresponding complex C_6H_6-HXeF.[28] In addition, we also studied the complexes of HArF and XH_2P (X = F, Cl, and Br) and found three stable complexes.[30] The pnicogen bond formed between the σ-hole (a region with positive electrostatic potentials) on the P atom of XH_2P and the F atom of HArF is stronger than the hydrogen bond formed between the H atom of HArF and the lone pair on the P atom, as well as the halogen bond formed between the F atom of HArF and the halogen atom X of XH_2P.[30] Recently, Bauzá and Frontera[31] proposed the term "aerogen bonding" to describe the σ-hole interaction between Lewis bases and the noble-gas atom and suggested that this interaction may act as a new supramolecular force in crystal materials.

In this paper, we studied the complexes formed between HArF and YH_3X (X = halogen, Y = C and Si) in order to present a detailed investigation of their stabilities, electronic structures, and vibrational frequencies using quantum chemical calculations. Each molecular pair can be combined via three different binding modes, including a hydrogen bond (HB), a halogen bond (XB), and a tetrel bond (TB). Tetrel bonding is a σ-hole interaction between a region of positive electrostatic potential on the outer surface of the tetrel atom and a neighbouring negative site. This interaction has been suggested to be important in crystal materials,[32-34] chemical

[a] The Laboratory of Theoretical and Computational Chemistry, School of Chemistry and Chemical Engineering, Yantai University, Yantai 264005, People's Republic of China. E-mail: liqingzhong1990@sina.com; Fax: +86 535 6902063; Tel: +86 535 6902063.
[b] Department of Biological and Chemical Sciences, The University of the West Indies, Cave Hill Campus, Barbados. E-mail: sacm@mail.com.
†Electronic Supplementary Information (ESI) available: [Figures S1 and S2]. See DOI: 10.1039/x0xx00000x

reactions,[35] and biological systems.[36] We first explain the formation of the three interactions based on molecular electrostatic potentials, then we compare the stability of the three different complexes via their interaction energies and investigate the stability of the complexes with an energy decomposition method. The vibrational frequency shift of the H–Ar stretch vibration was analyzed by considering orbital interactions and occupancies.

2. Theoretical methods

All calculations were carried out with the Gaussian 09 program.[37] The geometries of the complexes and the respective monomers were optimized at the MP2 level with the aug-cc-pVTZ basis set for all atoms except the iodine atom. The aug-cc-pVTZ-PP basis set was adopted for the iodine atom to account for relativistic effects. Harmonic frequency calculations were then performed at the same level to confirm that the obtained structures correspond to energy minima on the potential energy surfaces. The interaction energy was calculated as the difference between the energy of the complex and the energy sum of the respective monomers. The interaction energy was corrected for the basis set superposition error (BSSE) with the counterpoise method of Boys and Bernardi.[38]

The molecular electrostatic potential (MEP) of YH_3X (X = halogen, Y = C and Si) on the 0.001 electrons/bohr^3 contour of the electronic density were calculated at the MP2/aug-cc-pVTZ level with the wavefunction analysis–surface analysis suite (WFA-SAS) program.[39] The topological analysis for all complexes was performed by using Bader's theory of atoms in molecules (AIM) with the help of AIM2000 software.[40] Natural bond orbital (NBO) analysis[41] was carried out at the HF/aug-cc-pVTZ level via the procedures contained in Gaussian 09 to analyze orbital interactions, occupancy, and charge transfer. The GAMESS program[42] was used to perform an energy decomposition analysis for the interaction energy using the LMOEDA method[43] at the MP2/aug-cc-pVTZ level.

3. Results and discussion

3.1 MEPs of XH_3Y

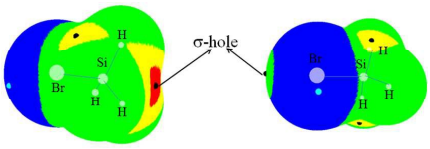

Fig. 1. MEP maps of SiH_3Br. Color ranges are: red, greater than 105; yellow, between 105 and 52; green, between 52 and 0; blue, less than 0. All are in kJ/mol

To gain an understanding of the interaction modes between YH_3X and HArF, we plotted the map of molecular electrostatic potentials (MEPs) of SiH_3Br in Fig. 1. A σ-hole is evident on the outer side of the Br atom along the Si-Br bond and this σ-hole is surrounded by the negative MEPs, corresponding to the lone pairs on the Br atom. As a result, it is reasonable to consider the σ-hole on the Br atom as the Lewis acid site for formation of a halogen bond with the F atom (Lewis base) of HArF and for the lone pair on the Br atom to act as the Lewis base for formation of a hydrogen bond with the proton of HArF. Simultaneously, four σ-holes are also observed at the tetrahedral face centers of SiH_3Br, in which the σ-hole along the Br–Si bond has a larger positive MEP (red region) than the other three σ-holes (yellow region) along the H–Si bond. Henceforth, we shall only focus on the larger σ-hole on the Si atom, which can form a tetrel bond with the F atom of HArF.

Table 1. The most positive MEPs (V_{max}, kJ/mol) on the σ-hole of the halogen and tetrel atoms as well as the most negative MEPs (V_{min}, kJ/mol) on the halogen atom in the molecules YH_3X (X = halogen; Y = C and Si).

	V_{max}(X)	V_{max}(Y)	V_{min}(X)
CH_3F	---	87.90	-95.71
CH_3Cl	2.07	73.46	-61.28
CH_3Br	27.04	66.88	-55.39
CH_3I	56.82	54.04	-46.72
SiH_3F	---	162.84	-86.59
SiH_3Cl	-5.94	150.62	-39.27
SiH_3Br	14.95	145.86	-35.06
SiH_3I	40.68	135.01	-29.41

Note: The MEP at the outer end of C-F bond in CH_3F is -92.34 kJ/mol.

The values of the related electrostatic potentials of YH_3X (X = halogen, Y = C and Si) are given in Table 1. No σ-hole is present on the F atom of CH_3F and SiH_3F, due to the fact that F has a greater electronegativity and lower polarizability than the other X (and Y) atoms. The most positive MEP on the halogen atom, V_{max}(X), becomes larger with increasing halogen atomic mass. When the C atom in CH_3X is replaced by Si, the value of V_{max}(X) is reduced and it even becomes negative on the Cl atom of SiH_3Cl, owing to the lower electronegativity of Si. On the other hand, the most negative MEP on the halogen atom, V_{min}(X), becomes less negative with an increase of halogen atomic number. The X atom in CH_3X shows a larger V_{min}(X) than that in SiH_3X although the C atom has a greater electronegativity than the Si atom. The most positive MEP on the Y atom, V_{max}(Y), becomes larger for the lighter X atom and the heavier Y atom. Importantly, V_{max}(Y) is much larger than V_{max}(X) except in CH_3I, indicating that the tetrel atom is a stronger Lewis acid than the halogen atom.

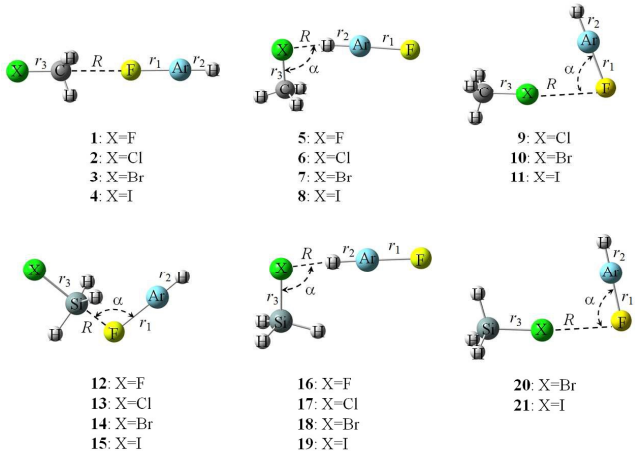

Fig. 2. Structures of tetrel-, hydrogen-, and halogen-bonded complexes

Table 2. Binding distance (R, Å), change of bond length (Δr, Å), and angle (α, deg) in the complexes of YH_3X-HArF (X = halogen; Y = C and Si).

	type	R	Δr_{Ar-F}	Δr_{H-Ar}	Δr_{X-Y}	α
1	TB	2.8271	0.0176	-0.0075	0.0108	180.0
2	TB	2.8172	0.0190	-0.0079	0.0119	180.0
3	TB	2.8032	0.0181	-0.0079	0.0096	180.0
4	TB	2.8353	0.0169	-0.0073	0.0076	180.0
5	HB	1.5374	0.1131	0.0063	0.0346	120.4
6	HB	1.9026	0.1143	0.0303	0.0171	94.5
7	HB	1.9951	0.1208	0.0432	0.0124	90.9
8	HB	2.1526	0.1243	0.0597	0.0064	87.7
9	XB	3.1979	0.0057	-0.0021	0.0008	76.7
10	XB	2.9200	0.0155	-0.0059	0.0027	86.8
11	XB	2.8178	0.0358	-0.0131	0.0092	94.1
12	TB	1.9735	0.1617	-0.0404	0.0581	103.3
13	TB	1.9032	0.2018	-0.0435	0.1389	103.5
14	TB	1.8770	0.2196	-0.0447	0.1674	103.2
15	TB	1.8497	0.2416	-0.0455	0.2074	103.0
16	HB	1.6754	0.0823	-0.0118	0.0333	180.0
17	HB	2.0093	0.0872	0.0122	0.0426	98.9
18	HB	2.0792	0.0977	0.0247	0.0433	93.3
19	HB	2.2132	0.1052	0.0432	0.0417	87.2
20	XB	3.1107	0.0102	-0.0035	-0.0030	84.0
21	XB	2.9653	0.0260	-0.0092	-0.0015	92.9

3.2 Structures and energetics

Fig. 2 shows the structures of complexes between YH_3X and HArF. The respective geometrical parameters are collected in Table 2. For the tetrel-bonded complexes of CH_3X (**1-4**), the molecule HArF is in line with the C–X bond, whereas for the tetrel-bonded complexes of SiH_3X (**12-15**), the molecule HArF is not in line with the Si–X bond, making an angle of about 103°. For the hydrogen-bonded complexes (**5-8** and **17-19**), the molecule HArF deviates from the line of the Y–X bond and this deviation is reduced with the increase of halogen atomic mass, consistent with the position of the most negative MEP on the halogen atomic surface. There is an exception for the hydrogen-bonded complex of SiH_3F-HArF (**16**), where the molecule HArF is collinear with the Si–F bond. This exception is due to the fact that the position of the most negative MEP on the F atom of SiH_3F is along the Si–F axis. In this collinear orientation, the interatomic repulsion between the F of SiH_3F and the Ar of HArF would be smaller than the corresponding repulsion between the X of SiH_3X (X = Cl, Br, and I) and the Ar of HArF (which would make this collinear orientation less favourable for these complexes with their heavier halogen X atoms). Also, the polarization of the heavier X atoms (by the large HArF dipole) in the side-on approach would be much greater for SiH_3X than for SiH_3F, thereby stabilizing the side-on complexes. The hydrogen-bonded complexes show C_s symmetry, but the molecule HArF is on the same side as one of the Si–H bonds in **17-19** and is on the opposite side to one of the C–H bonds in **5-8**. This geometrical feature is also found for the halogen-bonded complexes (**9-11** and **20-21**). The Ar atom of HArF is close to the X atom in the halogen-bonded complexes. Thus, there is a very weak contact between the positively charged Ar atom and the lone pair on the halogen atom, which is further confirmed by the subsequent AIM analyses. With the increase of X atomic number, the negative MEP on the X surface is decreased; thus this interaction is weakened, as characterized by a larger X···F–Ar angle.

Table 3. Interaction energy (kJ/mol) for the complexes of YH_3X-HArF (X = halogen; Y = C and Si) at the MP2 level with the different basis sets.

	type	Aug-cc-pVTZ	Aug-cc-pVQZ	CBS
1	TB	-16.28	-16.20	-16.16
2	TB	-16.44	-16.41	-16.40
3	TB	-16.13	-16.17	-16.19
4	TB	-14.88	-14.30	-14.03
5	HB	-31.17	-31.13	-31.11
6	HB	-31.49	-31.56	-31.59
7	HB	-32.08	-32.25	-32.33
8	HB	-32.98	-32.79	-32.70
9	XB	-6.19	-6.54	-6.70
10	XB	-10.68	-11.03	-11.19
11	XB	-19.75	-19.59	-19.52
12	TB	-108.27	-99.52	-95.47
13	TB	-136.75	-123.37	-117.18
14	TB	-149.30	-133.99	-126.90
15	TB	-162.99	-143.94	-135.12
16	HB	-25.94	-24.88	-24.39
17	HB	-23.42	-22.86	-22.60
18	HB	-24.98	-24.57	-24.38
19	HB	-27.23	-26.41	-26.03
20	XB	-7.81	-8.14	-8.29
21	XB	-14.36	-14.35	-14.35

The interaction energies of the three types of interactions in these complexes are listed in Table 3. The MP2 interaction energies are calculated with three different basis sets - aug-cc-pVTZ, aug-cc-pVQZ, and with the complete basis set (CBS) extrapolation. In particular, for most complexes, the MP2/aug-cc-pVQZ results are very close to those in the CBS limit, indicating that these calculated interaction energies were converged. An exception is found for the tetrel-bonded complexes of SiH_3X, which is attributed to the large deformation of SiH_3X in the complexes. It should be noted that the geometries of SiH_3X in the complexes were used to calculate the interaction energy of the tetrel-bonded complexes of SiH_3X (**12-15**). For the CH_3X complexes, the hydrogen-bonded complexes are most stable, while for the SiH_3X complexes, the tetrel-bonded complexes are most stable, followed by the hydrogen-bonded complexes, and the weakest complexes are the halogen-bonded complexes. Clearly, the stability of the complex is dependent on the nature of both the X and Y atoms. As expected, the halogen bond becomes stronger for the heavier halogen atoms and CH_3X is a stronger halogen donor than SiH_3X, showing a consistent change with the most positive MEP on the halogen atom. However, the hydrogen bond is also stronger for the heavier halogen atom with the exception in **16**, inconsistent with the most negative MEP on the halogen atom. This inconsistency indicates that the electrostatic interaction is not necessarily the only significant factor in determining the stability of hydrogen-bonded complexes. The interaction energy of the tetrel bond is almost the same in **1-3** although the most positive MEP on each carbon atom is clearly different. Moreover, the interaction energy of the tetrel bond in **12-15** becomes more negative with an increase of the halogen atomic number, which is inconsistent with the most positive MEP on the Si atom. This inconsistency may be

related to the deformation of SiH_3X in these complexes – notice that the normal tetrahedral geometry of SiH_3X, evident in **16-21**, is replaced by a trigonal bipyramidal geometry in **12-15**, in which the Si and the three H atoms are almost in the same plane.

The binding distance of the hydrogen bond becomes longer with an increase of the halogen atomic radius, while the reverse occurs for the binding distance of the halogen bond. The former change is inconsistent with the increase in the interaction energy, whereas the latter change is in agreement with the interaction energy trend. Thus the descriptive statement for the correlation between the interaction energy and the binding distance does not provide insightful arguments. It is noted that the binding distance is related to both the atomic radius and the interaction strength. The intermolecular separation (*R*) is substantially shorter in the hydrogen-bonded complexes compared with their halogen-bonded analogues, so the repulsion between SiH_3X and HArF becomes more pronounced in the hydrogen-bonded dimers and limits how closely the subunits approach each other in these dimers. This may be why the change in *R* with increasing size of X is inconsistent for the more strongly-bound hydrogen-bonded species. The binding distance of the tetrel bond shows an irregular change in the CH_3X complexes but shortens in the SiH_3X complexes as the interaction becomes stronger. The binding distance is about 1.85 Å in **15**, which is much shorter than the sum of the van der Waals radii of the respective atoms (about 3.57 Å)[44] but is longer than the covalent length of the F–Si bond (about 1.56 Å). This suggests that the tetrel bond in the SiH_3X complexes has some covalent character.

The increase in interaction energy (and corresponding decrease in binding distance) in **12-15** may be rationalized by considering that although the σ-hole arising from the Si atom of SiH_3X decreases going from X = F to I (Table 1), the polarizability of SiH_3X along the X-Si axis increases accordingly. Consequently, the dipole moment induced in SiH_3X (along the X-Si axis) due to the electric field of the highly polar FArH molecule, will increase as X gets larger. This induced dipole can then interact favourably with the F lone pair of FArH oriented along the X-Si molecular axis. The large X-Si bond extension (increasing from F to I, Table 2) would also enhance the dipole-dipole interaction between SiH_3X and FArH. We also note that in **12-15**, the negatively charged H atoms of the SiH_3 subunit (H is more electronegative than Si) all lie in the same plane so as to minimize the repulsion between these H atoms and the X and F (of FArH) lone pairs.

Whether for the associated bond in the halogen- and tetrel-bonded complexes or for the free bond in the hydrogen-bonded complexes, the ionic Ar–F bond is elongated in all complexes. In general, the elongation of the Ar–F bond correlates well with the interaction strength. Accordingly, the largest elongation of the Ar–F bond is found in the tetrel-bonded complexes of SiH_3X. The associated H–Ar bond is lengthened in the hydrogen-bonded complexes, whereas the distant H–Ar bond is shortened in the halogen- and tetrel-bonded complexes. There is an exception for the hydrogen-bonded complex of SiH_3F-HArF (**16**), where the H–Ar bond is compressed. The elongation of the H–Ar bond in the hydrogen bond shows some dependence on the interaction strength, but a prominent change with the increase of X atomic number is evident, in spite of the small change in the interaction energy. Also the contraction of the distant H–Ar bond correlates well with the strength of the halogen and tetrel bonds. The X–Y bond is stretched in all complexes except in the halogen-bonded complexes of SiH_3Br-HArF (**20**) and SiH_3I-HArF (**21**), in which a contraction occurs for the X–Y bond. Again, the largest stretching of X–Y bond is found in the tetrel-bonded complexes of SiH_3X (**12-15**).

3.3 Frequency shifts

It is well-known that the H–Z stretch vibration usually exhibits a red shift in most hydrogen bonds, although there are also blue-shifting hydrogen bonds. The frequency shifts of Ar–F, H–Ar, and X–Y stretch vibrations are summarized in Table 4. Generally, these shifts are consistent with the change of the respective bond length. The Ar–F stretch vibration exhibits a red shift in all complexes, showing a coincident change in the strength of the corresponding interaction.

Table 4. Frequency shifts of selected stretch vibrations ($\Delta\nu$, cm^{-1}) in the complexes of XH_3Y-HArF (X = halogen; Y = C and Si).

	type	$\Delta\nu_{Ar-F}$	$\Delta\nu_{H-Ar}$	$\Delta\nu_{X-Y}$
1	TB	-13	77	-35
2	TB	-14	80	-28
3	TB	-13	80	-19
4	TB	-13	74	-13
5	HB	-98	-78	-99
6	HB	-106	-333	-38
7	HB	-115	-445	-25
8	HB	-123	-598	-15
9	XB	-6	18	1
10	XB	-15	54	2
11	XB	-25	90	1
12	TB	-97	434	-138
13	TB	-139	472	-129
14	TB	-165	486	-339
15	TB	-169	496	-496
16	HB	-76	153	-81
17	HB	-87	-140	-45
18	HB	-103	-268	-27
19	HB	-101	-454	-31
20	XB	-10	32	3
21	XB	-25	90	1

The H–Ar stretch vibration also displays a red shift in the hydrogen-bonded complexes except in **16**. The red shift of the H–Ar stretch vibration in the hydrogen-bonded complexes of YH_3X-HArF is the reverse of the blue shift of the H–Ar stretch vibration observed in the complexes of HArF with H_2, N_2, CO, and CO_2.[1-10] In the previous study for the frequency shift of the H–Ar stretch vibration, we found that it could be regulated by cooperative effects.[10] We therefore infer that the red shift of the H–Ar stretch vibration in **5-8** and **17-19** is mainly due to the stronger hydrogen bond. Interestingly, the red shift of the H–Ar stretch vibration is strongly dependent on the nature of halogen atom although the corresponding interaction energies do not change significantly. This result is helpful in distinguishing the hydrogen bond formed by HArF with different molecules YH_3X by means of infrared spectroscopy. On the other hand, the H–Ar stretch vibration shows a blue shift in the tetrel- and halogen-bonded complexes. This

distant blue shift was also observed for other complexes of HArF.[11] Moreover, it appears to be closely linked to the interaction strength. The largest blue shift (496 cm^{-1}) is found in the tetrel-bonded complex of SiH_3I-HArF, which is larger than the value obtained for the halogen-bonded complexes of HArF and dihalogen molecule,[11] but smaller than the values for the beryllium-bonded complexes of HArF and BeH_2.[45] It is noted that the distant blue shift of the H–Ar stretch vibration is also large enough to be detected with experimental methods, perhaps by matrix isolation techniques.

In previous studies, a strong correlation was found between bond length change/frequency shift and the chemical "hardness" of the proton acceptor Y in X–H···Y complexes.[46,47] In this model, the red shift is correlated with decreasing hardness (or increasing polarizability) of the atom to which the H is bonded, while a blue shift is correlated with increasing hardness.[46,47] This model may explain the increasing H–Ar red shift (and bond elongation) for SiH_3X-HArF dimers (**17-19**) and the H–Ar blue shift (and bond compression) in SiH_3F-HArF (**16**). Note that the polarizability along the Si–F axis will be the smallest (and the F atom, the hardest) in the latter dimer, favouring an H–Ar blue shift. This should be compared with the side-on SiH_3X-HArF dimers, for which the hardness decreases with increasing size of X (Cl > Br > I) and the polarizability (as measured by the polarizability components perpendicular to the Si–X bond axis) increases accordingly, favouring a steadily increasing red shift (and bond elongation) for these complexes.

The X–Y stretch vibration exhibits a red shift in the tetrel- and hydrogen-bonded complexes, while its shift is very small in the halogen-bonded complexes. Furthermore, the red shift of the X–Y stretch vibration becomes smaller with the increase of X atomic mass in **1-8** and **16-19**, due to the heavier mass of the X atom. However, this red shift increases going from SiH_3Cl to SiH_3I in the tetrel-bonded complexes of SiH_3X-HArF. We ascribe this tendency to the stronger tetrel bond.

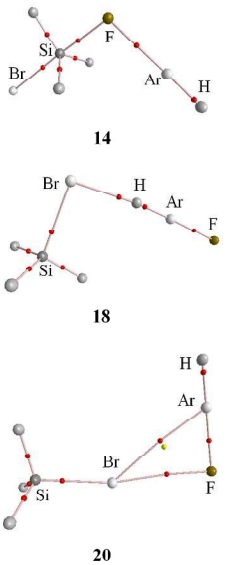

Fig. 3. Molecular maps of tetrel- (**14**), hydrogen- (**18**), and halogen (**20**) -bonded complexes of SiH_3Br-HArF.

3.4 AIM analyses

Fig. 3 shows the molecular maps of the complexes between HArF and SiH_3Br. The existence of tetrel, hydrogen, and halogen bonds is characterized by Si···F, H···Br, and Br···F bond critical points (BCPs), respectively. In the halogen-bonded complex **20**, there is also a Br···Ar BCP, providing an evidence for a weak $Br^-\cdots Ar^+$ interaction. Since Kr has a larger positive charge in HKrF than Ar does in HArF, it is expected that a Br···Kr BCP (corresponding to a stronger $Br^-\cdots Kr^+$ interaction) should be obtained for the analogous $SiH_3Br\cdots$HKrF complex, which has been confirmed in Fig. S1. Actually, the $Br^-\cdots Ar^+$ interaction is also present in the halogen-bonded complex **7** since the Br atom in CH_3Br has a larger V_{min}(Br) than that in SiH_3Br. This interaction in **7** and **20** can be evidenced by the non-covalent interactions (NCI) map in Fig. S2, where a green area is observed between the Br and Ar atoms. The electron density, Laplacian, and energy density at these BCPs are collected in Table 5. The electron density ranges from 0.006 to 0.067 au in the complexes, which is partly in the range 0.002-0.04 au as suggested for hydrogen bonds by Koch and Popelier.[48] The electron density in **4-8** and **12-19** is out of this range, suggesting the presence of stronger interactions in these complexes. The electron density at the Y···F BCP increases with an increase of X atomic mass, which disagrees with the interaction energy trend for the C···F tetrel bond, but agrees with the interaction energy trend for the Si···F tetrel bond. The electron densities in the hydrogen and halogen bonds are not compared due to the different types of BCP. The value of the Laplacian at the Si···F BCP is much larger than those for the other BCPs. The energy density is negative for **4-8** and **12-19**, but is positive for the other complexes. The positive energy density corresponds to a predominantly closed-shell interaction,[49] whereas the negative energy density means that the corresponding interaction has a partially covalent character.[49]

Table 5. Electron density (ρ, au), Laplacian ($\nabla^2\rho$, au), and energy density (*H*, au) at the intermolecular BCP in the complexes.

	type	ρ	$\nabla^2\rho$	*H*
1	TB	0.0081	0.0459	0.0022
2	TB	0.0087	0.0475	0.0023
3	TB	0.0092	0.0487	0.0023
4	TB	0.0095	0.0441	0.0019
5	HB	0.0562	0.1302	-0.0159
6	HB	0.0529	0.0310	-0.0189
7	HB	0.0535	0.0120	-0.0195
8	HB	0.0538	0.0115	-0.0158
9	XB	0.0060	0.0268	0.0013
10	XB	0.0126	0.0534	0.0018
11	XB	0.0192	0.0756	0.0018
12	TB	0.0493	0.2719	-0.0051
13	TB	0.0585	0.3628	-0.0054
14	TB	0.0624	0.4039	-0.0056
15	TB	0.0669	0.4513	-0.0058
16	HB	0.0365	0.1210	-0.0042
17	HB	0.0400	0.0482	-0.0102
18	HB	0.0430	0.0316	-0.0123
19	HB	0.0428	0.0162	-0.0121
20	XB	0.0093	0.0372	0.0014
21	XB	0.0152	0.0580	0.0017

3.5 NBO analyses

The interactions in these complexes have also been analyzed by considering the orbital interactions. It was found that there is an orbital interaction of $Lp_F \rightarrow BD^*_{X-Y}$ in the tetrel and halogen bonds but $Lp_X \rightarrow BD^*_{H-Ar}$ in the hydrogen bond. The orbital interaction $Lp_F \rightarrow BD^*_{X-Y}$ was not found in **12-15** due to the formation of a Si–F bond. These orbital interactions are estimated using the second-order perturbation energies in Table 6. One can see that the hydrogen bond has a strong orbital interaction, characterized by large perturbation energies. For the hydrogen bond, the strong orbital interaction also reflects a sizeable covalent contribution. The perturbation energy of the $Lp_X \rightarrow BD^*_{H-Ar}$ orbital interaction has a similar trend to that for the interaction energy of the hydrogen bond, but the former trend is more prominent than the latter. The perturbation energy is smaller in **1-4**, **9-11**, and **20-21**, and is also consistent with the trend for the interaction energy of the halogen bond.

Table 6. Second-order perturbation energy (E^2, kJ/mol), sum of charge on all the atoms of HArF (q_{HArF}, e), and differences between NBO electron density (ED) in the complexes and in the isolated HArF in the H–Ar sigma bonding ($\Delta\sigma$) and sigma anti-bonding ($\Delta\sigma^*$) orbitals.

	type	E^2	q_{HArF}	$\Delta\sigma_{H-Ar}$	$\Delta\sigma^*_{H-Ar}$
1	TB	6.19	0.0040	0.0000	-0.0117
2	TB	7.06	0.0056	-0.0001	-0.0123
3	TB	7.86	0.0063	-0.0001	-0.0123
4	TB	7.34	0.0061	-0.0001	-0.0116
5	HB	172.13	-0.0582	-0.0014	0.0007
6	HB	291.76	-0.1323	0.0002	0.0728
7	HB	354.46	-0.1685	0.0002	0.1075
8	HB	404.41	-0.2097	0.0011	0.1486
9	XB	2.47	0.0034	-0.0002	-0.0026
10	XB	13.12	0.0090	-0.0003	-0.0081
11	XB	35.03	0.0189	-0.0003	-0.0190
12	TB	---	0.1360	-0.0030	-0.0621
13	TB	---	0.1619	-0.0025	-0.0702
14	TB	---	0.1706	-0.0023	-0.0733
15	TB	---	0.1793	-0.0021	-0.0766
16	HB	74.70	-0.0268	-0.0010	-0.0199
17	HB	187.77	-0.0847	0.0000	0.0369
18	HB	252.43	-0.1201	0.0010	0.0682
19	HB	302.30	-0.1596	0.0011	0.1053
20	XB	4.60	0.0038	-0.0003	-0.0052
21	XB	15.17	0.0106	-0.0003	-0.0138

Note: E^2 corresponds to the orbital interaction of $Lp_F \rightarrow BD^*_{X-Y}$ in TB and XB, $Lp_X \rightarrow BD^*_{H-Ar}$ in HB.

The sum of the atomic charges on HArF (q_{HArF}) is also given in Table 6. The q_{HArF} value is negative for the hydrogen bond but positive for the tetrel and halogen bonds. With the increase of halogen atomic mass, q_{HArF} becomes more negative or positive in all complexes, except in **4**. This indicates that the charge transfer is important in the formation of these complexes. The magnitude of charge transfer is particularly large in **4-8** and **12-19**.

Upon complexation, the charge densities in the H–Ar bonding and anti-bonding orbitals are changed. One can see in Table 6 that the charge density in the H–Ar bonding orbital changes only slightly but for the H–Ar anti-bonding orbital, relatively large changes are obtained. Specifically, the charge density in the H–Ar anti-bonding orbital is decreased in the tetrel and halogen bonds, while it is increased in the hydrogen bond except in **16**. The decrease of charge density in the H–Ar anti-bonding orbital leads to an enhancement of the H–Ar bond, leading to the contraction of the H–Ar bond and a blue shift. On the other hand, the increase of charge density in the H–Ar anti-bonding orbital results in a weakening of the H–Ar bond, being responsible for its elongation and corresponding red shift.

3.6 Energy decomposition analyses

To gain a better understanding of the origin of the stability of these complexes, the interaction energy was decomposed into five components: the electrostatic energy (ES), exchange energy (EX), repulsion energy (REP), polarization energy (POL), and dispersion energy (DISP).[43] The corresponding results are presented in Table 7. The interaction energies in Tables 3 and 7 are almost equal for most complexes except **5-8, 11**, and **15-19**. The reason for their deviations is that the optimized geometries of the monomers are used in Table 3 used to compute the interaction energies in Table 3, whereas the geometries that the monomers adopt in the optimized complexes are used to compute the interaction energies in Table 7. It is expected that the electrostatic energy is largest for the stronger halogen bond in **11** and **21**. For the moderate halogen bond in **10** and **20**, the three attractive terms of ES, POL and DISP make comparable contributions. However, DISP makes a larger contribution than ES to the weak halogen bond in **9**.

Table 7. Electrostatic energy (ES), exchange energy (EX), repulsion energy (REP), polarization energy (POL), and dispersion energy (DISP) in the complexes at the MP2/aug-cc-pVTZ level. All quantities are in kJ/mol.

	ES	EX	REP	POL	DISP
1	-23.37	-19.86	32.94	-5.85	-0.46
2	-22.82	-22.91	37.95	-7.44	-1.38
3	-22.82	-24.87	41.17	-8.32	-1.13
4	-20.15	-24.20	39.79	-8.90	-1.17
5	-79.80	-99.32	194.70	-57.43	3.18
6	-61.70	-116.66	223.96	-77.66	-7.02
7	-60.99	-126.90	244.49	-88.74	-8.44
8	-53.21	-130.79	250.63	-99.69	-10.58
9	-6.06	-18.39	31.64	-4.60	-8.86
10	-18.81	-42.93	74.15	-10.78	-12.50
11	-45.31	-83.14	145.26	-23.62	-14.21
12	-277.89	-360.27	694.21	-160.34	-4.56
13	-340.75	-425.19	831.28	-204.03	1.00
14	-368.72	-454.20	892.60	-224.47	4.89
15	-405.04	-495.71	979.25	-250.93	10.62
16	-58.06	-58.14	111.90	-32.23	5.73
17	-43.26	-84.98	160.89	-53.88	-8.11
18	-45.65	-100.32	191.15	-66.84	-10.07
19	-41.93	-109.39	207.79	-79.67	-12.62
20	-10.45	-28.76	48.86	-7.23	-10.41
21	-29.85	-61.49	105.46	-16.55	-12.67

ES contributes more to the stability of the tetrel-bonded complexes than POL and DISP in **1-4**. Moreover, the ES term has a

consistent change with the most positive MEP on the C atom. For the tetrel bond in **12-15**, there is a large EX, which corresponds to a substantial overlap between the molecular orbitals, evidenced by the strong orbital interactions. This large EX is accompanied by a large REP due to the close contact between the two molecules, as confirmed by the shorter binding distances. The ES term is also larger than the POL term in **12-15**, although both contributions are quite large. The large POL contribution means that the orbitals undergo a significant change in their shapes, which is typical for the formation of a covalent bond. In addition, both ES and POL terms become more negative with an increase of halogen atomic number. The results above show that the tetrel bond is dominated by the electrostatic interaction but nonetheless also exhibits the characteristics of a covalent interaction. It is also found that **12-15** show substantially larger ES than the other complexes, consistent with the relatively larger positive MEP on the Si atom than on the C and halogen atoms.

For the hydrogen bond, with the increase of halogen atomic number, ES is less negative but POL is more negative. The POL contribution exceeds that of ES in most hydrogen bonds. The decrease of ES accords with the change of the most negative MEP on the halogen atom. Therefore, the hydrogen bond is governed by a combination of electrostatic and polarization energies, and the polarization contribution even exceeds that of the electrostatic energy in most cases. Additionally, the contributions from EX and REP should not be ignored. DISP is positive in **5** and **13-16**, which is unfavorable for the stability of these complexes. The positive dispersion energy in these complexes is caused by the differences in the intra- and interionic correlation energy on going from noninteracting to interacting molecules.[43] It has been shown that the dispersion energy is sensitive to the binding distance,[43] from the positive one to the negative one when the distance is longer. The binding distance is very short in these complexes, being responsible for the positive DISP.

4. Conclusions

A theoretical study of the tetrel-, hydrogen-, and halogen-bonded complexes formed by HArF with YH_3X (X = halogen, Y = C and Si) has been undertaken by means of ab initio MP2 computational methods. The energetic results show that the HB complexes are favored in the CH_3X complexes while the TB complexes are the most stable of the SiH_3X complexes. Interestingly, most complexes become more stable with an increase of the halogen atomic mass.

The vibrational analysis of these complexes showed a significant red shift of the H–Ar bond, between 78-598 cm^{-1}, in the hydrogen-bonded complexes, whereas a sizeable blue shift was found in the complexes with halogen bond and tetrel bonds. These shifts have a pronounced change when the halogen is varied, particularly in the hydrogen-bonded complexes, although the interaction energy only changes slightly. Consequently, it should be possible for these complexes to be detected and distinguished using spectroscopic methods, perhaps by matrix isolation techniques.

The NBO and AIM analyses showed that the tetrel bond in the SiH_3X complexes and the hydrogen bond in all complexes have a partially covalent nature. The energy decomposition analyses indicated that the interactions above are jointly governed by electrostatic and polarization forces. The relative contribution of each energy component to the stability of the halogen bond is apparently dependent on how strong the halogen bond is.

Acknowledgements

This work was supported by the National Natural Science Foundation of China (21573188).

References

1. M. Solimannejad and I. Alkorta, *Chem. Phys. Lett.*, 2007, **439**, 284–287.
2. S. A. C. McDowell, *Chem. Phys.*, 2004, **301**, 53–60.
3. S. A. C. McDowell, *Chem. Phys. Lett.*, 2003, **368**, 649–653.
4. S. A. C. McDowell, *Mol. Phys.*, 2004, **102**, 71–77.
5. S. A. C. McDowell, *Chem. Phys. Lett.*, 2005, **406**, 228–231.
6. M. Solimannejad and I. Alkorta, *Chem. Phys.*, 2006, **324**, 459–464.
7. A.V. Nemukhin, B. L. Grigorenko, L. Khriachtchev, H. Tanskanen, M. Pettersson and M. Räsänen, *J. Am. Chem. Soc.*, 2002, **124**, 10706–10711.
8. S.A.C. McDowell, *J. Chem. Phys.*, 2005, **122**, 204309.
9. H. Tanskanen, S. Johansson, A. Lignell, L. Khriachtchev and M. Räsänen, *J. Chem. Phys.*, 2007, **127**, 54313.
10. X.F. Liu, Q.Z. Li, J.B. Cheng and W.Z. Li, *Mol. Phys.*, 2013, **111**, 497–504.
11. Q.Z. Li, Z.B. Liu, B. Jing, W.Z. Li, J.B. Cheng, B.A. Gong and J.Z. Sun, *Spectrochimica Acta A*, 2010, **77**, 506–511.
12. L. Khriachtchev, M. Pettersson, N. Runeberg, J. Lundell and M. Räsänen, *Nature (London)*, 2000, **406**, 874–876.
13. L. Khriachtchev, M. Pettersson, A. Lignell and M. Räsänen, *J. Am. Chem. Soc.*, 2001, **123**, 8610–8611.
14. M. Pettersson, L. Khriachtchev, A. Lignell, M. Räsänen, Z. Bihary and R. B. Gerber, *J. Chem. Phys.*, 2002, **116**, 2508–2515.
15. L. Graham, O. Graudejus, N. K. Jha and N. Bartlett, *Coord. Chem. Rev.*, 2000, **197**, 321–334.
16. J. J. Turner and G. C. Pimentel, *Science*, 1963, **140**, 974–975.
17. D. S. Brock, V. Bilir, H. P. A. Mercier and G. J. Schrobilgen, *J. Am. Chem. Soc.*, 2007, **129**, 3598–3611.
18. L. Khriachtchev, K. Isokoski, A. Cohen, M. Räsänen and R. B. Gerber, *J. Am. Chem. Soc.*, 2008, **130**, 6114–6118.
19. L. Khriachtchev, H. Tanskanen, J. Lundell, M. Pettersson, H. Kiljunen and M. Räsänen, *J. Am. Chem. Soc.*, 2003, **125**, 4696–4697.
20. J. Lundell and M. Pettersson, *Phys. Chem. Chem. Phys.*, 1999, **1**, 1691–1697.
21. J. Lundell, S. Berski and Z. Latajka, *Phys. Chem. Chem. Phys.*, 2000, **2**, 5521–5527.
22. A. V. Nemukhin, B. L. Grigorenko, L. Khriachtchev, H. Tanskanen, M. Pettersson and M. Räsänen, *J. Am. Chem. Soc.*, 2002, **124**, 10706–10711.
23. S.A.C. McDowell, *Phys. Chem. Chem. Phys.*, 2003, **5**, 808–811.
24. S.A.C. McDowell, *Chem. Phys.*, 2004, **301**, 53–60.
25. A. Lignell, J. Lundell, L. Khriachtchev and M. Räsänen, *J. Phys. Chem. A*, 2008, **112**, 5486–5494.
26. S.A.C. McDowell, *J. Chem. Phys.*, 2004, **121**, 5728–5732.
27. M. Solimannejad and A. Boutalib, *Chem. Phys.*, 2006, **320**, 275–280.
28. X.F. Liu, Q.Z. Li, R. Li, W.Z. Li and J.B. Cheng, *Spectrochimica Acta A*, 2011, **84**, 68–73.
29. Q.Z. Li, J.L. Zhao, R. Li, W.Z. Li, J.B. Cheng and B.A. Gong, *Comput. Theor. Chem.*, 2011, **970**, 61–65.
30. X.F. Liu, J.B. Cheng, Q.Z. Li and W.Z. Li, *Spectrochimica Acta A*, 2013, **101**, 172–177.

31. A. Bauzá and A. Frontera, *Angew. Chem. Int. Ed.*, 2015, **54**, 7340–7343.
32. A. Bauzá, T. J. Mooibroek and A. Frontera, *Angew. Chem. Int. Ed.*, 2013, **52**, 12317–12321.
33. S.B. Choi, B.K. Kim, P. Boudjouk and D.G. Grier, *J. Am. Chem. Soc.*, 2001, **123**, 8117–8118.
34. N.W. Mitzel and U. Losehand, *Angew. Chem. Int. Ed.*, 1997, **36**, 2807–2809.
35. S. J. Grabowski, *Phys. Chem. Chem. Phys.*, 2014, **16**, 1824–1834.
36. D. Mani and E. Arunan, *Phys. Chem. Chem. Phys.*, 2013, **15**, 14377–14383.
37. M. J. Frisch, G. W. Trucks, H. B. Schlegel, G. E. Scuseria, M. A. Robb, J. R. Cheeseman, J. A. Montgomery Jr, T. Vreyen, K. N. Kudin, J. C. Burant, J. M. Millam, S. S. Iyengar, J. Tomasi, V. Barone, B. Mennucci, M. Cossi, G. Scalmani, N. Rega, G. A. Petersson, H. Nakatsuji, M. Hada, M. Ehara, K. Toyota, R. Fukuda, J. Hasegawa, M. Ishida, T. Nakajima, Y. Honda, O. Kitao, H. Nakai, M. Klene, X. Li, J. E. Knox, H. P. Hratchian, J. B. Cross, C. Adamo, J. Ja ramillo, R. Gomperts, R. E. Stratmann, O. Yazyev, A. J. Austin, R. Cammi, C. Pomelli, J. W. Octhterski, P. Y. Ayala, K. Morokuma, G. A. Voth, P. Salvador, J. J. Dannenberg, V. G. Zakrzewski, S. Dapprich, A. D. Daniels, M. C. Strain, O. Farkas, D. K. Malick, A. D. Rabuck, K. Raghavachari, J. B. Foresman, J. V. Ortiz, Q. Cui, A. G. Baboul, S. Clifford, J. Cioslowski, B. B. Stefanov, G. Liu, A. Liashenko, P. Piskorz, I. Komaromi, R. L. Martin, D. J. Fox, T. Keith, M. A. Al Laham, C. Y. Peng, A. Nanayakkara, M. Challacombe, P. M. W. Gill, B. Johnson, W. Chen, M. W. Wong, C. Gonzalez and J. A. Pople, Gaussian 09, Revision A.02, Gaussian, Inc., Wallingford CT, 2009.
38. S.F. Boys and F. Bernardi, *Mol. Phys.*, 1970, **19**, 553–566.
39. F.A. Bulat, A. Toro-Labbé, T. Brinck, J.S. Murray and P. Politzer, *J. Mol. Model.*, 2010, **16**, 1679–1691.
40. R. F. W. Bader, *AIM2000 Program, v 2.0*, McMaster University, Hamilton, Canada, 2000.
41. A.E. Reed, L.A. Curtiss and F.A. Weinhold, *Chem. Rev.*, 1988, **88**, 899–926.
42. M. W. Schmidt, K. K. Baldridge, J. A. Boatz, S. T. Elbert, M. S. Gordon, J. H. Jensen, S. Koseki, N. Matsunaga, K. A. Nguyen, S. J. Su, T. L. Windus, M. Dupuis and J. A. Montgomery, *J. Comput. Chem.*, 1993, **14**, 1347–1363.
43. P. F. Su and H. Li, *J. Chem. Phys.*, 2009, **13**, 014102.
44. A. Bondi, *J. Phys. Chem.*, 1964, **68**, 441–451.
45. Q.Z. Li, X.F. Liu, R. Li, J.B. Cheng and W.Z. Li, *Spectrochimica Acta A*, 2012, **90**, 135–140.
46. A.D. Buckingham, J.E. Del Bene and S.A.C. McDowell, *Chem. Phys. Lett.*, 2008, **463**, 1–10.
47. S.A.C. McDowell and A. J. Thakkar, *Int. J. Quantum Chem.*, 2010, **110**, 1506–1513.
48. U. Koch and P. L. A. Popelier, *J. Phys. Chem. A*, 1995, **99**, 9747–9754.
49. W. D. Arnold and E. Oldfield, *J. Am. Chem. Soc.*, 2000, **122**, 12835–12841.

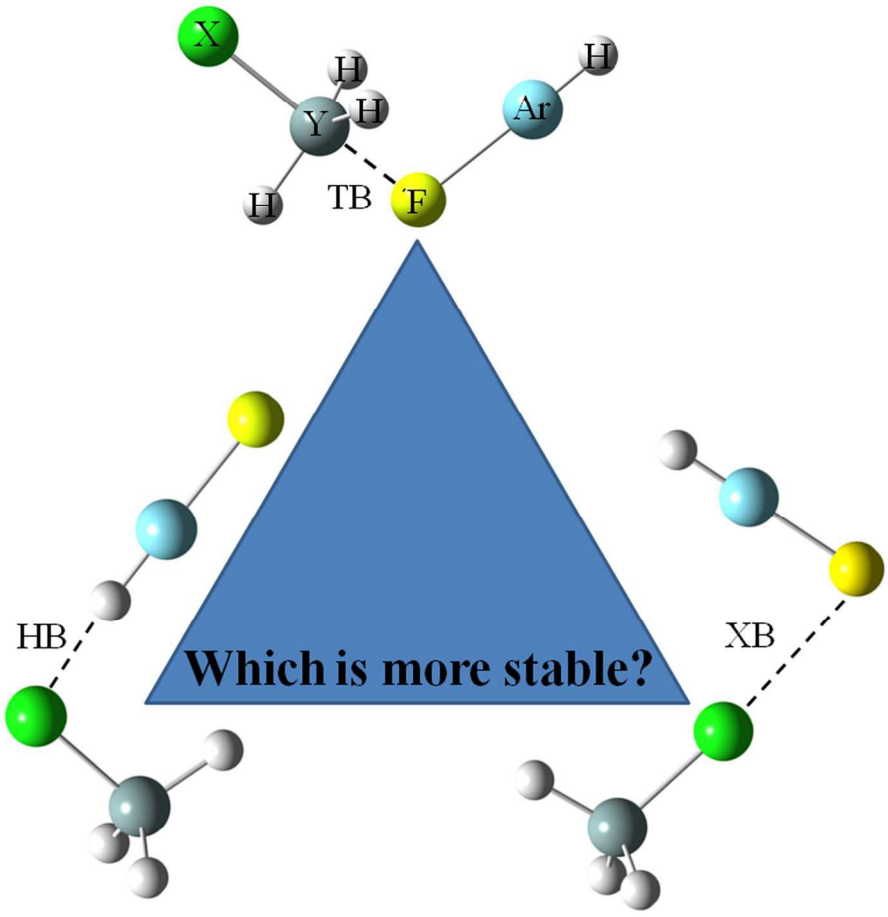

74x69mm (600 x 600 DPI)